Micron 63 (2014) 57–63

Contents lists available at ScienceDirect

Micron

journal homepage: www.elsevier.com/locate/micron

The effect of probe inaccuracies on the quantitative model-based analysis of high angle annular dark field scanning transmission electron microscopy images

G.T. Martinez[a,*], A. De Backer[a], A. Rosenauer[b], J. Verbeeck[a], S. Van Aert[a]

[a] Electron Microscopy for Materials Science (EMAT), University of Antwerp, Gronenborgerlaan 171, 2020 Antwerp, Belgium
[b] Institut für Festkörperphysik, Universität Bremen, Otto-Hahn-Alle 1, D-28359 Bremen, Germany

ARTICLE INFO

Article history:
Received 20 September 2013
Received in revised form
13 December 2013
Accepted 15 December 2013
Available online 27 December 2013

Keywords:
HAADF STEM
Probe aberrations
Statistical parameter estimation theory
STEM simulations

ABSTRACT

Quantitative structural and chemical information can be obtained from high angle annular dark field scanning transmission electron microscopy (HAADF STEM) images when using statistical parameter estimation theory. In this approach, we assume an empirical parameterized imaging model for which the total scattered intensities of the atomic columns are estimated. These intensities can be related to the material structure or composition. Since the experimental probe profile is assumed to be known in the description of the imaging model, we will explore how the uncertainties in the probe profile affect the estimation of the total scattered intensities. Using multislice image simulations, we analyze this effect for *Cs* corrected and non-*Cs* corrected microscopes as a function of inaccuracies in cylindrically symmetric aberrations, such as defocus and spherical aberration of third and fifth order, and non-cylindrically symmetric aberrations, such as 2-fold and 3-fold astigmatism and coma.

1. Introduction

The use of a high angle annular dark field detector in a scanning transmission electron microscope (HAADF STEM) allows one to obtain images whose contrast is sensitive to structural and chemical information of the material under study. The intensities of these images scale with the mean atomic number Z of the atomic columns, hence the name Z-contrast imaging (Pennycook and Jesson, 1991). It has also been demonstrated that the intensities can be related to the number of atoms present in each atomic column (Van Aert et al., 2011, 2013; LeBeau et al., 2010; De Backer et al., 2013). Therefore, this technique is widely used for chemical and structural analyses of materials at the atomic level. To analyze HAADF STEM images as accurately and precisely as possible, quantitative methods are needed. In order to analyze HAADF STEM images quantitatively, several approaches have been proposed (Rosenauer et al., 2009; Robb et al., 2012; LeBeau et al., 2008; Kotaka, 2010). Furthermore, statistical parameter estimation theory has been introduced as an alternative method to extract quantitative information from HAADF STEM images, such as chemical composition (Van Aert et al., 2009; Martinez et al., 2014) or number of atoms (Van Aert et al., 2011, 2013; De Backer et al., 2013), with high accuracy and precision. In this framework, HAADF STEM images are described using a simplified parameterized empirical imaging model. The unknown parameters of this model are then estimated in an iterative way by fitting this model to the experimental images using a criterion of goodness of fit, such as least squares, least absolute squares or maximum likelihood (den Dekker et al., 2005; Van Aert et al., 2005). In this manner, the total intensity of scattered electrons can be quantified atomic column-by-atomic column, which is particularly interesting due to its sensitivity for the chemical composition. The use of this methodology has been shown to allow for a chemical quantification of interfaces (Van Aert et al., 2009), and to study the structure and composition of nanoparticles (Bals et al., 2011) and nanoclusters (Bals et al., 2012). The research on nanostructured materials such as nanoparticles is of great interest because of their wide applications in different fields, such as catalysts for example (Yu et al., 2012). Model-based quantification of HAADF STEM images has been presented in Van Aert et al. (2009, 2012) and an extensive analysis on the inherent limitations of this methodology as a tool for atom counting has been explained in De Backer et al. (2013). Furthermore, the model assumptions and validity for single atomic column chemical quantification have been discussed in Martinez et al. (2014). In this work, we analyze how inaccuracies in the probe aberrations, which are usually assumed to be known, affect the estimation of the scattered intensities of the atomic columns. For that purpose, we will make use of multislice simulations under the absorptive potential

* Corresponding author. Tel.: +32 (0) 32653317.
E-mail address: gerardo.martinez@uantwerpen.be (G.T. Martinez).

0968-4328/$ – see front matter © 2013 Elsevier Ltd. All rights reserved.
http://dx.doi.org/10.1016/j.micron.2013.12.009

approach (Ishizuka, 2002) because of their suitability to describe electron-sample interactions for thin samples. In Section 2, we will review the model-based analysis for quantification of HAADF STEM images. In Section 3 we will describe the simulation methodology and settings. We consider the example of Pt as a test material because of its increasing interest in the catalyst research community (Chen and Holt-Hindle, 2010). However, the analysis can be extended to all types of materials. In Section 4, the results will be presented and discussed. Finally, in Section 5, conclusions are drawn.

2. Model-based parameter estimation

Model-based electron microscopy has recently been reviewed in Van Aert et al. (2012), where a wide scope of applications is discussed as well. For the particular case of quantification of *Z*-contrast HAADF STEM images, the methodology is presented in Van Aert et al. (2009). Quantitative information is then obtained by measuring total scattered atom column intensities using statistical parameter estimation theory. An empirical incoherent imaging model is used to measure these quantities. This parametric model describes the expectations of the pixel values of the HAADF STEM image. If we assume an incoherent model for this purpose, we can describe the electron-sample interaction as the convolution between an object function and the probe intensity (Pennycook and Jesson, 1991; Nellist, 2007):

$$f_{kl}(\boldsymbol{\theta}) = f(\mathbf{r}_{k,l};\boldsymbol{\theta}) = \mathrm{O}(\mathbf{r}_{k,l};\boldsymbol{\theta}) * \mathrm{P}(\mathbf{r}_{k,l}) \tag{1}$$

where $\mathrm{O}(\mathbf{r};\boldsymbol{\theta})$ is the object function depending on the unknown structure parameters $\boldsymbol{\theta}$ and $\mathrm{P}(\mathbf{r})$ is the probe function depending on a set of probe parameters including acceleration voltage, defocus, aperture semi-angle, spherical aberration constant and high order aberration coefficients. The indices (k, l) correspond to the STEM probe at position $\mathbf{r}_{k,l} = (x_k\, y_l)^T$.

The information about the sample and the HAADF detector is incorporated in the object function, which describes the scattering interaction of the probe with the projected potential recorded at the detector plane. This function is sharply peaked at the atom column positions and can be defined as a superposition of Gaussian peaks:

$$\mathrm{O}(\mathbf{r}_{k,l};\boldsymbol{\theta}) = \zeta + \sum_{n=1}^{N} \eta_n \exp\left(\frac{-(x_k-\beta_{x_n})^2-(y_l-\beta_{y_n})^2}{2\rho^2}\right) \tag{2}$$

where ζ is a constant background, N is the total number of atomic columns to be analyzed, ρ is the width of a Gaussian peak, η_n is the height of the nth Gaussian peak, β_{x_n} and β_{y_n} are the x- and y-coordinates of the nth atomic column, respectively.

Thus, the unknown parameters are given by the parameter vector:

$$\boldsymbol{\theta} = (\beta_{x_1}, \ldots, \beta_{x_N}, \beta_{y_1}, \ldots, \beta_{y_N}, \rho, \eta_1, \ldots, \eta_N, \zeta)^T \tag{3}$$

In order to estimate the unknown parameters, use is made of the uniformly weighted least squares estimator. The function parameters are then estimated by minimizing the least squares sum using an iterative routine. After the estimation of the unknown parameters from the experimental images, the volumes under the Gaussian peaks above the background are used as a sensitive measure to extract quantitative information. It has been shown that this measure is proportional to the total intensity of electrons scattered by a specific atomic column that was integrated at the HAADF detector (Van Aert et al., 2009). These volumes can be computed as follows:

$$\mathrm{V}_n = 2\pi\eta_n\rho^2 \tag{4}$$

The function $\mathrm{P}(\mathbf{r})$ in Eq. (1) is the STEM probe that scans over the sample. It is given by the following expression:

$$\mathrm{P}(\mathbf{r}) = |p(\mathbf{r})|^2 * S(\mathbf{r}) \tag{5}$$

where $|p(\mathbf{r})|^2$ is the coherent point source contribution and $S(\mathbf{r})$ represents the incoherent source size effects (Born and Wolf, 1998). The STEM probe formation takes place at the objective lens, which strongly focuses the electron beam to form a crossover which is described by the function $p(\mathbf{r})$. This function is given by the inverse Fourier transform of the transfer function of the objective lens $T(\mathbf{g})$, which is defined as:

$$T(\mathbf{g}) = A(\mathbf{g})\exp(i\chi(\mathbf{g})) \tag{6}$$

with $A(\mathbf{g})$, the so-called aperture function, being a circular top-hat function with unity height and radius g_{ap}. The objective aperture semi-angle α_0 is related to this function by the equality $\alpha_0 = g_{ap}\lambda$, where λ is the electron wavelength. The exponential term in Eq. (6) describes a phase shift $\chi(\mathbf{g})$ due to the objective lens aberrations. The function $\chi(\mathbf{g})$ incorporates the effect of rotationally symmetric aberrations, such as defocus and spherical aberration of third and fifth order. Non-symmetric aberrations such as astigmatism and coma can also be included in this function for a more accurate description of the probe profile (Haider et al., 2000). Extensive work has been performed in order to measure the objective lens aberrations (Haider et al., 2000; Wong et al., 1992; Uhlemannm and Haider, 1998; Batson, 2006; Krivanek et al., 2008). The most recent aberration corrected instruments incorporate automated routines to measure the residual aberrations on a daily basis. Computer assisted routines have been developed to analyze diffractogram tableaus, so-called Zemlin-tableaus (Zemlin et al., 1978), and to address residual aberrations and their stability during the experiment (Barthel and Thust, 2010). For STEM, use is made of far-field shadow images, so-called Ronchigrams, to perform this task (Lupini et al., 2010). The parametric model proposed in Van Aert et al. (2009) assumes the probe function to be known. This probe function is determined by the instrument. The characteristic probe aberrations should be measured experimentally. Residual aberrations can be measured with different methodologies up to the unavoidable experimental limitations, including reading noise, fluctuations of the probe current due to microscope instabilities, hardware and software computational restrictions (Barthel and Thust, 2010). Thus, there is an unavoidable uncertainty in the probe profile. Therefore, we will study how these inaccuracies affect the parameter estimates, the scattered intensities given by Eq. (4), in particular. We will show our analysis as a function of inaccuracies in defocus (C_1), spherical aberration of third (C_3) and fifth order (C_5), 2-fold (A_1) and 3-fold (A_2) astigmatism and coma (B_2).

3. HAADF STEM simulation study

The analysis presented in this work will make use of multislice simulations under the absorptive potential approximation (Ishizuka, 2002) using the StemSim software (Rosenauer and Schowalter, 2007). The absorptive potential approximation is computationally less demanding while it still describes the image intensities properly up to 50 nm thickness of the sample (Rosenauer et al., 2009). We simulated a Pt structure in [1 0 0] and [1 1 0] zone axis up to 75 atoms thickness, that is, ≈30 nm and ≈21 nm, respectively. The simulated images were convolved with a Gaussian function to account for spatial incoherence. We consider two cases: a *Cs* corrected and a non-*Cs* corrected microscope under their corresponding Scherzer conditions. The simulation settings are summarized in Table 1.

Using the theory described in Section 2, the scattered intensities, given by Eq. (4), have been estimated from the simulated images

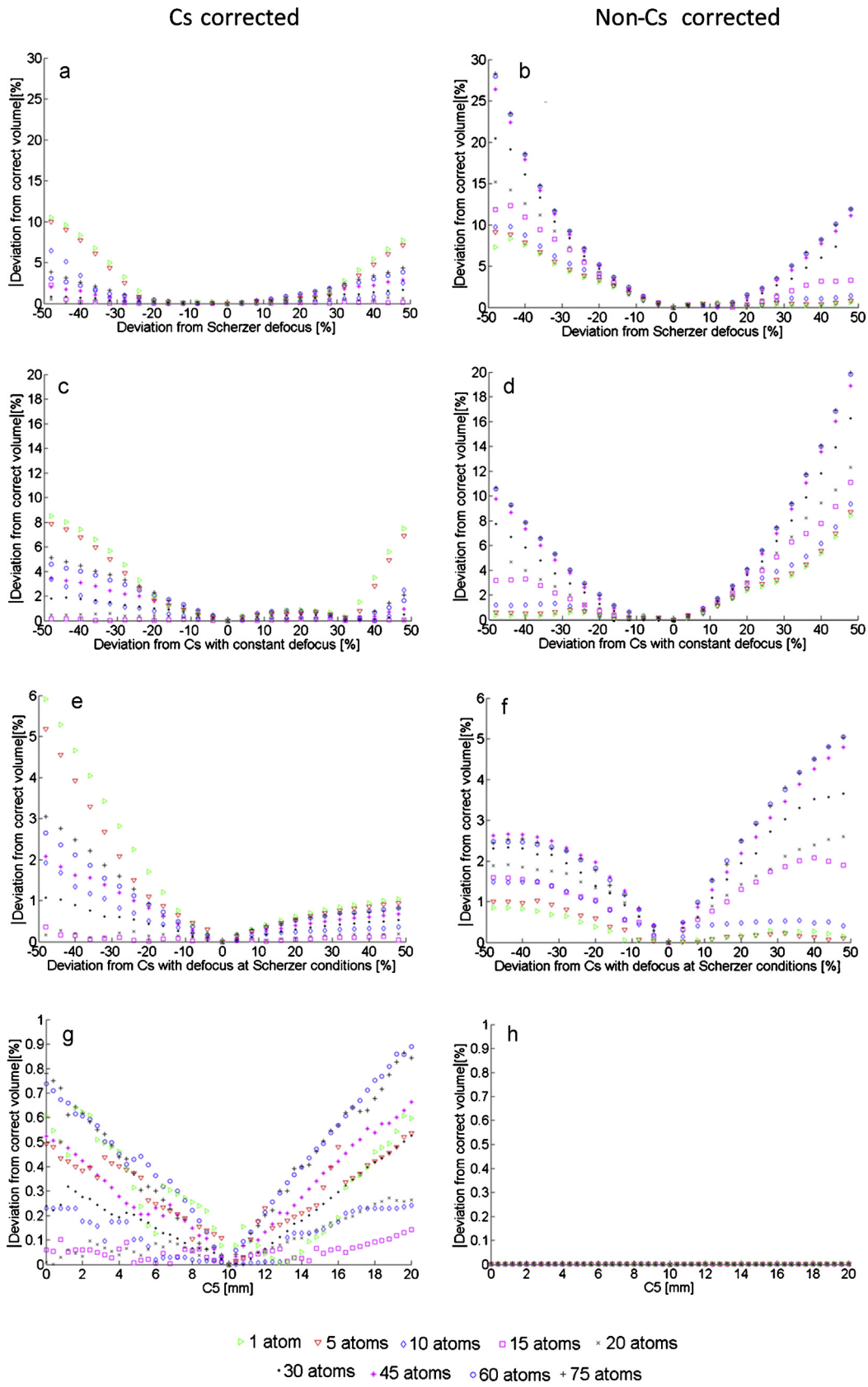

Fig. 1. Percentage of deviation in total scattered intensity (estimated volume given by Eq. (4)) as a function of probe inaccuracies for Pt in [1 0 0] zone axis. (a and b) Deviations as a function of defocus while keeping *Cs* and C_5 constant. (c and d) Deviations as a function of *Cs* while keeping Scherzer defocus and C_5 constant. (e and f) Deviations as a function of *Cs* while adapting defocus to meet Scherzer conditions. C_5 is kept constant. (g and h) Deviations as a function of C_5 while keeping defocus and *Cs* constant.

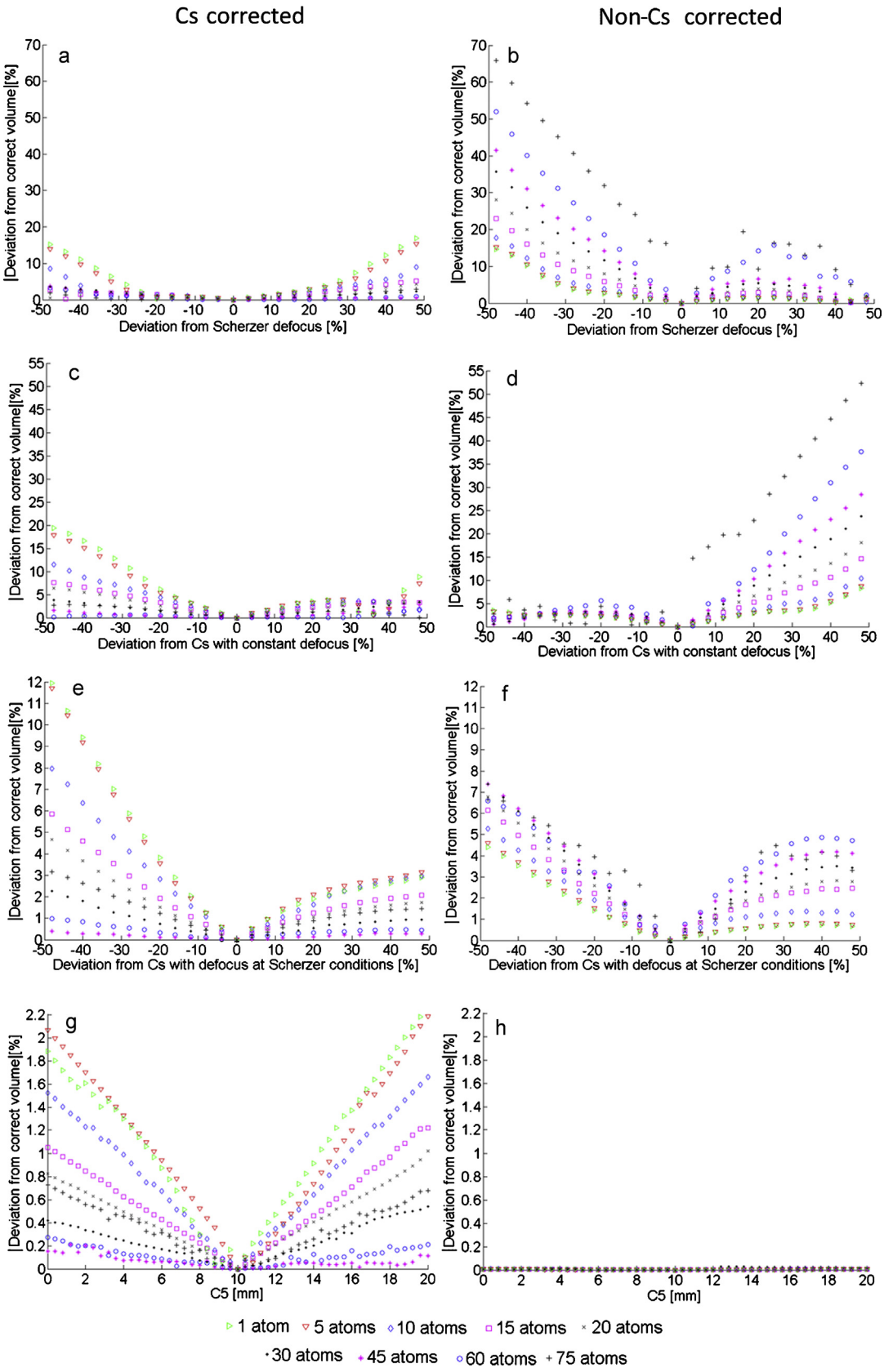

Fig. 2. Percentage of deviation in total scattered intensity (estimated volume given by Eq. (4)) as a function of probe inaccuracies for Pt in [1 1 0] zone axis. (a and b) Deviations as a function of defocus while keeping *Cs* and C_5 constant. (c and d) Deviations as a function of *Cs* while keeping Scherzer defocus and C_5 constant. (e and f) Deviations as a function of *Cs* while adapting defocus to meet Scherzer conditions. C_5 is kept constant. (g and h) Deviations as a function of C_5 while keeping defocus and *Cs* constant.

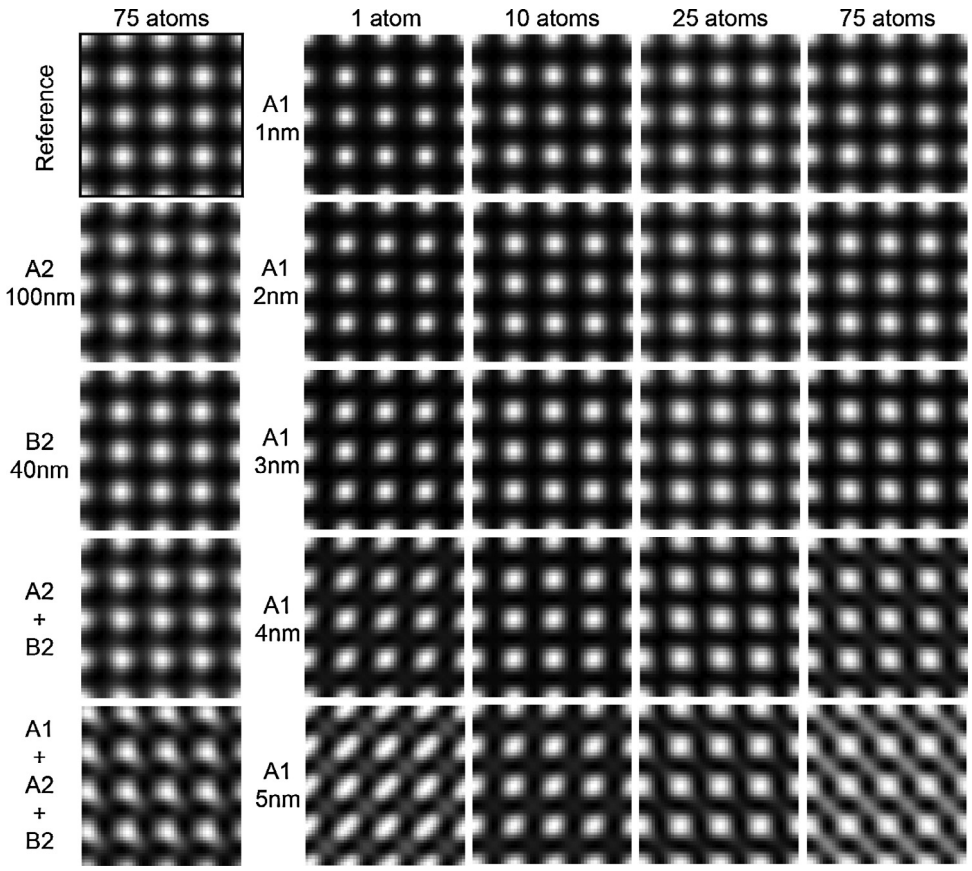

Fig. 3. Simulated images when considering different non-cylindrically symmetric aberrations. Reference image is simulated taking into account simulation settings described in Table 1. Reference, A_2, B_2, $A_2 + B_2$ and $A_1 + A_2 + B_2$ images are shown for 75 atom thickness. Sum of A_1, A_2 and B_2 considered values of 5 nm, 100 nm and 40 nm, respectively. Images including A_1 for 1 to 5 nm are shown for 1, 10, 25 and 75 atoms thickness. When A_1 is present, the distortion of the image is dependent on the amount of aberration and the sample thickness. The shape of the atomic column deviates from a rounded shape. When A_2 and B_2 are considered, the shape of the atomic column can still be modeled by rounded Gaussians. The effect of A_1 is predominant in respect to A_2 and B_2.

assuming variation in the probe aberrations around the true aberrations. As presented in Martinez et al. (2014), fitting a constant background to simulations is not needed, since this background considers the signals that do not originate from the sample under study, such as the sample support or the grid. Consequently, a background with value 0 was considered for this analysis. Furthermore, we will study the effect on the scattered intensities for 1, 5, 10, 15, 20, 30, 45, 60 and 75 atoms thickness. The analysis of simulated images for two different zone axes is intended to consider different atomic column spacings, having a different effect on the cross-talk of the electron beam through the sample. Typical values for the non-cylindrically symmetric aberrations have been considered in the image simulations resulting from computer assisted alignment of the probe corrector in a FEI Titan cubed 80–300 kV. Regularly, values of 2-fold astigmatism (A_1) below 5 nm are obtained. For 3-fold (A_2) astigmatism and coma (B_2), the amount of aberration used is 100 nm and 40 nm, respectively. These aberrations considered a rotation angle of $\pi/4$.

Table 1
Settings used for multislice simulations.

Microscope	*Cs* corrected/non-*Cs* corrected
Acceleration voltage HT	300 kV
Defocus C_1	−8.8741 nm/−48.606 nm
Spherical aberration C_3	0.04 mm/1.2 mm
Spherical aberration C_5	10 mm
Objective aperture angle α	21.1 mrad/9 mrad
Spatial incoherence of source FWHM	0.7 Å/1.23 Å
Number of unit cells per supercell	9×9
HAADF inner collection angle	60 mrad
HAADF outer collection angle	190 mrad
Maximum specimen thickness [1 0 0]	29.4 nm
Maximum specimen thickness [1 1 0]	20.8 nm
Debye–Waller factor B	0.384 Å^2
Pixel size [1 0 0]	0.1569 Å
Pixel size [1 1 0]	0.1121 Å
Non-cylindrically symmetric aberrations:	
2-Fold astigmatism (A_1)	1–5 nm at $\pi/4$
3-Fold astigmatism (A_2)	100 nm at $\pi/4$
Coma (B_2)	40 nm at $\pi/4$

4. Results and discussion

4.1. Analysis of cylindrically symmetric aberrations

The analysis for cylindrically symmetric aberrations is presented in Figs. 1 and 2, where the effect of variations around the true aberration coefficients on the total scattered column intensities is shown. Figs. 1 and 2(a and b) show the deviations of total scattered intensity in percentage with respect to variation of defocus from Scherzer defocus conditions for a *Cs* corrected and non-*Cs* corrected microscope, respectively. Negative and positive deviations are considered corresponding to underfocus and overfocus, respectively. All other microscope settings are given in Table 1. For the *Cs* corrected instrument, it follows that a variation in defocus of ±20% results in a deviation of ≈1% regardless the number of atoms present in the sample or zone axis. For larger variations, the deviation increases significantly and depends on the number of atoms,

resulting in a higher deviation when few atoms are present. In the non-*Cs* corrected example, the effect of the variation in defocus is more pronounced and highly dependent on atomic column spacing, that is, the chosen zone axis. For the [1 0 0] zone axis, the deviation reaches ≈5% for a variation of ±20%. For [1 1 0] zone axis, the same amount of variation in defocus leads to a deviation up to ≈30% for large number of atoms. Figs. 1 and 2(c and d) show the deviation of the total scattered intensity as a function of variations in *Cs* while keeping the defocus value constant. In this case, a ±20% variation around the true *Cs* value leads to a deviation of ≈2% in [1 0 0] zone axis and ≈5% in [1 1 0] for the *Cs* corrected microscope. Higher deviations are found for the non-*Cs* corrected example when a larger number of atoms is present. In comparison with Figs. 1 and 2(e and f), where the defocus is adapted to meet Scherzer conditions with varying *Cs*, the deviation in total scattered intensities is significantly smaller. The deviation is less than ≈4% in the ±20% defocus variation range regardless of number of atoms, zone axis or *Cs* correction. Finally, Figs. 1 and 2(g and h) show the effect of varying C_5. These results indicate very small deviations in total scattered intensities for a range of ±10 *mm* around the true C_5. However, deviations are larger for the *Cs* corrected microscope as compared to the non-*Cs* corrected microscope. Modification of the probe profile due to this aberration is indeed more prominent in case of *Cs* correction. For the case of the non-*Cs* corrected microscope, the effect is practically none regardless of zone axis, due to the predominant effect of *Cs* aberration on the probe profile. An overall observation of this study is that *Cs* correction is more sensitive to inaccuracies in the probe settings for a few number of atoms. Estimated scattered intensities obtained from images of a non-*Cs* corrected microscope are clearly affected with respect to the number of atoms present in the crystal and atomic column spacing. However, deviations in estimated scattered intensities ≈ 1 to 5% are observed when the experimental uncertainties in the true probe settings are in the ±20% range for most cases. The quantification of scattered intensities is less affected when the probe profile is significantly peaked. This demonstrates a robust behavior of this model-based method with respect to probe inaccuracies for cylindrically symmetric aberrations.

4.2. Analysis of non-cylindrically symmetric aberrations

As explained in Section 2, the proposed model considers only cylindrically symmetric aberrations, such as defocus and spherical aberrations of third (*Cs*) and fifth (C_5) order. However, in *Cs* corrected microscopes, the remaining non-cylindrically symmetric aberrations, such as 2-fold (A_1), 3-fold (A_2) astigmatism and coma (B_2), can have an important effect on the image, which is seldomly observed in non-*Cs* corrected instruments, because of the predominant effect of *Cs*. Therefore, we analyze how these aberrations affect estimated scattered intensities when taking images with a *Cs* corrected microscope. We compare the scattered intensities obtained at Scherzer conditions using the simulations settings from Table 1 for the [1 0 0] zone axis. Maximum values of 2-fold, 3-fold astigmatism and coma corresponding to typical values obtained when using computer assisted software to align the probe corrector in a Titan cubed 80–300 kV are considered for the simulations. Usually, values of A_1 should be below 5 nm when the corrector is properly aligned. This aberration is corrected at the moment of recording the image and it may even slightly vary during the acquisition. Consequently, we simulated a series of images including this aberration in 1 nm steps, ranging from 1 to 5 nm. The simulated images are shown in Fig. 3. Deviations from a rounded shape of the atomic column are observed depending on the amount of 2-fold astigmatism, but also depending on the number of atoms present. Fig. 4(a) shows the deviation from the estimated scattered intensity with respect to number of atoms for the different values of A_1. When comparing

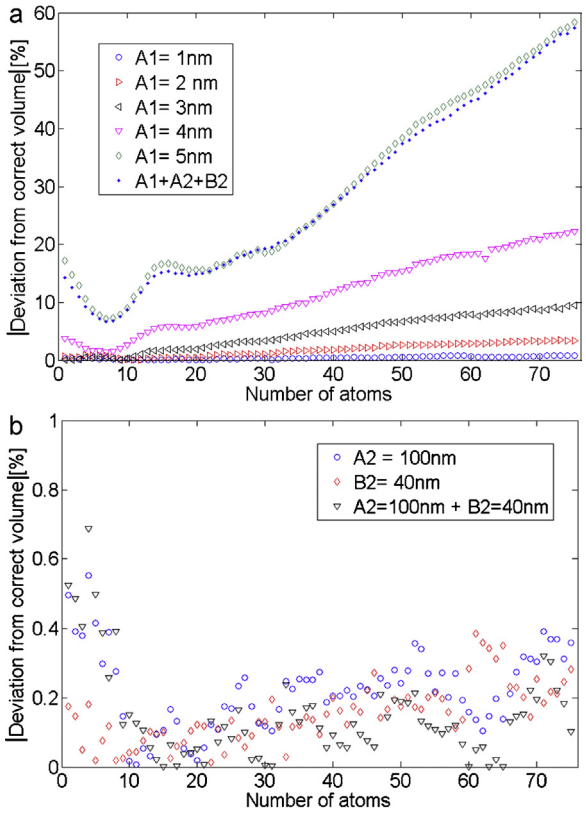

Fig. 4. Percentage of deviation in total scattered intensity (estimated volume given by Eq. (4)) as a function of number of atoms. (a) Deviation from correct volume when 2-fold A_1 astigmatism is included for 1–5 nm. Sum of A_1, A_2 and B_2 for 5 nm, 100 nm and 40 nm, respectively, is also shown. There is a predominant effect of A_1. (b) Deviation from correct volume when 3-fold A_2 astigmatism and coma B_2, is considered for 100 nm and 40 nm, respectively.

these results with the images shown in Fig. 3, it can be concluded that the deviation with respect to the reference case remains very small as long as the column shape is visually round. For values of A_1 up to 3 nm, the fitting procedure is able to retrieve most of the atomic column intensity even when considering a Gaussian shape to model the column images. In contrast, for 5 nm 2-fold astigmatism, deviations are large indicating the need to correct for this aberration manually after using computer assisted software. Special attention is drawn to the case of 10 atoms thickness showing a minimum in the deviation. In Fig. 3, the nearly rounded shape of the atomic column is observable at this thickness, corresponding to the turning point of the asymmetry of the column. For values below 10 atoms, the asymmetry direction is observed indeed from lower left to upper right of the image, whereas for larger number of atoms, the asymmetry direction changes from lower right to upper left of the image. This observation is expected due to the asymmetry of the probe profile while propagating inside the crystal. Fig. 3 also shows simulated images when A_2 and B_2 are included for 75 atoms thickness. For these aberrations, the deviation of a rounded shape is less prominent at the maximum values usually obtained after software correction, that is at 100 nm and 40 nm, respectively. Fig. 4(b) shows that the deviation from the reference scattered intensity when considering these aberrations separately or combined is less than 1%. Finally, a simulated image considering the maximum values (5 nm – 100 nm – 40 nm) for the three aberrations A_1, A_2 and B_2 together is shown in Fig. 3 for 75 atoms thickness. The combined aberrations result in a clearly distorted image. It is found that the effect of A_1 predominates and that the deviation with respect to the scattered intensity reference is very similar to the curve for 5 nm 2-fold

astigmatism in Fig. 4. In conclusion, the parametric model shows a robust behavior for non-cylindrically symmetric aberrations even if they are not taken into account in the probe profile.

5. Conclusions

Statistical parameter estimation theory has been shown to be a reliable technique to extract quantitative structural and chemical information from HAADF STEM images. This approach relies on estimating unknown structure parameters of an empirical parameterized imaging model. From these estimated parameters, the total scattered intensity of the atomic columns can be determined. The total scattered intensity is then related to structure or composition of the atomic column. In this approach, it is generally assumed that the scanning probe profile is known. In this work, we have explored how experimental uncertainties of the probe affect the estimated total scattered intensity. Using multislice simulations under Scherzer conditions, we have analyzed this effect for a *Cs* and non-*Cs* corrected microscope as a function of uncertainties in cylindrically symmetric aberrations, such as defocus and spherical aberration of third and fifth order for two different atomic column spacings. In general, it can be concluded that deviations in scattered intensities are between ≈1 and 5% when the experimental uncertainties are in the ±20% range for most cases. Reduced atomic column spacing and increasing number of atoms may have an important effect for non-*Cs* corrected instruments, whereas the scattered intensities for a *Cs* corrected instrument are more affected for few atoms present in the sample. Moreover, when adapting defocus for a varying *Cs* in order to keep Scherzer conditions, the deviations are clearly reduced. The effect of C_5 can practically be neglected for a non-*Cs* corrected microscope and has very little influence for the *Cs* corrected case. Since the model only considers cylindrically symmetric aberrations while estimating the model parameters, we analyzed how non-cylindrically symmetric aberrations, such as 2-fold and 3-fold astigmatism and coma, affect the estimation of the scattered intensities for a *Cs* corrected instrument, since for a non-*Cs* corrected microscope, the effect of these aberrations is overruled by the rounded distortion caused by *Cs*. It can be concluded that for typical aberration values for 3-fold astigmatism and coma after software correction, the shape of the atomic columns can still be modeled by a rounded Gaussian function and therefore, the deviation from the correct scattered intensity is less than ≈1%. The effect of 2-fold astigmatism depends on specimen thickness and the magnitude of the aberration. Up to values of 3 nm for A_1, deviations from the correct volume are below ≈10% for large number of atoms (75 atoms) and less than ≈5% for fewer atoms (less than 25 atoms).

In conclusion, the model-based analysis of HAADF STEM images is shown to be robust for inaccuracies in both cylindrically symmetric and non-cylindrically symmetric aberrations.

Acknowledgments

The authors acknowledge financial support from the Research Foundation Flanders (FWO, Belgium) through project fundings G.0393.11, G.0064.10, G.0374.13, G.0044.13 and a Ph.D. research grant to A.D.B.

J.V. was supported by funding from the European Research Council under the 7th Framework Program (FP7), ERC Grant No. 246791-COUNTATOMS and ERC Starting Grant No. 278510-VORTEX. A.R. thanks the DFG under contract number RO2057/8-1.

The research leading to these results has received funding from the European Union 7th Framework Programme [FP7/2007–2013] under grant agreement no. 312483 (ESTEEM2).

References

Bals, S., Casavola, M., Van Huis, M., Van Aert, S., Batenburg, K., Van Tendeloo, G., Vanmaekelbergh, D., 2011. Three-dimensional atomic imaging of colloidal core–shell nanocrystals. Nanoletters 11, 3420–3424.

Bals, S., Van Aert, S., Romero, C., Lauwaet, K., Van Bael, M., Schoeters, B., Partoens, B., Yücelen, E., Lievens, P., Van Tendeloo, G., 2012. Atomic scale dynamics of ultrasmall germanium clusters. Nature Communications 3, 897.

Barthel, J., Thust, A., 2010. Aberration measurement in HRTEM: implementation and diagnostic use of numerical procedures for highly precise recognition of diffractogram patterns. Ultramicroscopy 111, 27–46.

Batson, P., 2006. Characterizing probe performance in the aberration corrected stem. Ultramicroscopy 106, 1104–1114.

Born, M., Wolf, E., 1998. Principles of Optics-Electromagnetic Theory of Propagation, Interference and Diffraction of Light, seventh (expanded) ed. Cambridge University Press, Cambridge.

Chen, A., Holt-Hindle, P., 2010. Platinum-based nanostructured materials: synthesis, properties and applications. Chemical Reviews 110, 3767–3804.

De Backer, A., Martinez, G.T., Rosenauer, A., Van Aert, S., 2013. Atom counting in HAADF STEM using a statistical model-based approach: methodology, possibilities, and inherent limitations. Ultramicroscopy 134, 23–33.

den Dekker, A.J., Van Aert, S., van den Bos, A., Van Dyck, D., 2005. Maximum likelihood estimation of structure parameters from high resolution electron microscopy images. Part I: A theoretical framework. Ultramicroscopy 104, 83–106.

Haider, M., Uhlemann, S., Zach, J., 2000. Upper limits for residual aberrations of high-resolution aberration-corrected stem. Ultramicroscopy 81, 163–175.

Ishizuka, K., 2002. A practical approach for STEM image simulation based on the FFT multislice method. Ultramicroscopy 90, 71–83.

Kotaka, Y., 2010. Essential experimental parameters for quantitative structure analysis using spherical aberration-corrected HAADF-STEM. Ultramicroscopy 110, 555–562.

Krivanek, O., Corbin, G., Dellby, N., Elston, B., Keyse, R., Murfitt, M., Own, C., Szilagyi, Z., Woodruff, J., 2008. An electron microscope for the aberration-corrected era. Ultramicroscopy 108, 179–195.

LeBeau, J., Findlay, S., Allen, L., Stemmer, S., 2008. Quantitative atomic resolution scanning transmission electron microscopy. Physical Review Letters 100, 206101.

LeBeau, J., Findlay, S., Allen, L., Stemmer, S., 2010. Standardless atom counting in scanning transmission electron microscopy. Nanoletters 10, 4405.

Lupini, A., Wang, P., Nellist, P., Kirkland, A., Pennycook, S., 2010. Aberration measurement using the Ronchigram contrast transfer function. Ultramicroscopy 110, 891–898.

Martinez, G.T., Rosenauer, A., De Backer, A., Verbeeck, J., Van Aert, S., 2014. Quantitative composition determination at the atomic level using model-based high-angle annular dark field scanning transmission electron microscopy. Ultramicroscopy 137, 12–19.

Nellist, P., 2007. Scanning transmission electron microscopy. In: Hawkes, P.W., Spence, J.C.H. (Eds.), In: Science of Microscopy, vol. I. Springer, New York.

Pennycook, S., Jesson, D., 1991. High-resolution *Z*-contrast imaging of crystals. Ultramicroscopy 37, 14–38.

Robb, P., Finnie, M., Longo, P., Craven, A., 2012. Experimental evaluation of interfaces using atomic-resolution high angle annular dark field (HAADF) imaging. Ultramicroscopy 114, 11–19.

Rosenauer, A., Schowalter, M., 2007. STEMSIM—a new software tool for simulation of STEM HAADF *Z*-contrast imaging. Springer Proceedings in Physics 120, 169–172.

Rosenauer, A., Gries, K., Mueller, K., Pretorious, A., Schowalter, M., Avramescu, A., Engl, K., Lutgen, S., 2009. Measurement of specimen thickness and composition in $Al_xGa_{1-x}N$/GaN using high-angle annular dark field images. Ultramicroscopy 109, 1171–1182.

Uhlemannm, S., Haider, M., 1998. Residual wave aberrations in the first spherical aberration corrected transmission electron microscope. Ultramicroscopy 72, 109–119.

Van Aert, S., den Dekker, A.J., van den Bos, A., Van Dyck, D., Chen, J., 2005. Maximum likelihood estimation of structure parameters from high resolution electron microscopy images. Part II: A practical example. Ultramicroscopy 104, 107–125.

Van Aert, S., Verbeeck, J., Erni, R., Bals, S., Luysberg, M., Van Dyck, D., Van Tendeloo, G., 2009. Quantitative atomic resolution mapping using high-angle annular dark field scanning transmission electron microscopy. Ultramicroscopy 109, 1236–1244.

Van Aert, S., Batenburg, K., Rossel, M., Erni, R., Van Tendeloo, G., 2011. Three-dimensional atomic imaging of crystalline nanoparticles. Nature 470, 374–377.

Van Aert, S., Van den Broek, W., Goos, P., Van Dyck, D., 2012. Model-based electron microscopy: from images toward precise numbers for unknown structure parameters. Micron 43, 509–515.

Van Aert, S., De Backer, A., Martinez, G.T., Goris, B., Bals, S., Van Tendeloo, G., Rosenauer, A., 2013. Procedure to count atoms with trustworthy single-atom sensitivity. Physical Review B 87, 064107.

Wong, K., Kirlkland, E., Xu, P., Loane, R., Silcox, J., 1992. Measurement of spherical aberration in stem. Ultramicroscopy 40, 139–150.

Yu, W., Porosoff, M., Chen, J., 2012. Review of Pt-based bimetallic catalysis: from model surfaces to supported catalysts. Chemical Reviews, http://dx.doi.org/10.1021/cr300096b.

Zemlin, F., Weiss, K., Schiske, P., Kunath, W., Herrmann, K., 1978. Coma-free alignment of high resolution electron microscopes with the aid of optical diffractograms. Ultramicroscopy 3, 49–60.